RESEARCH ARTICLE
doi: 10.2306/scienceasia1513-1874.2026.098

ScienceAsia 52 (5): 2026: ID 2026098: **1–13**

Nuclear translocation of PD-L1 enhances anti-breast cancer immunity induced by tumor cell lysate

Yue Sun, Liu-Hui Ge, Xiu-Ting Ma, Bo-Han Dong*

Department of Microbiology and Immunology, Wannan Medical College, Wuhu, Anhui 241000 China

*Corresponding author, e-mail: 20100044@wnmc.edu.cn

Received 12 Oct 2025, Accepted 29 Sep 2026
Available online 12 Nov 2026

ABSTRACT: Programmed death-ligand 1 (PD-L1), a key ligand of the immune checkpoint receptor programmed cell death 1 (PD-1), is highly expressed in tumor cells and is also present in tumor cell lysates (TCL). TCL-based strategies have gained significant attention in anti-tumor immunity research in recent years. However, the heterogeneous composition of TCL complicates its immunomodulatory mechanisms. Nuclear translocation of tumor cell-derived PD-L1 may alter TCL immunogenicity and affect TCL-induced antitumor responses. To investigate this, doxorubicin was used to induce PD-L1 nuclear translocation in three breast cancer cell lines, and TCL containing nuclear-translocated PD-L1 (PT-TCL) was prepared. PT-TCL and TCL from normal breast cancer cells (PN-TCL) were then applied to T lymphocytes *in vitro* to assess the immune activity of PT-TCL and its differences from PN-TCL. Compared with PN-TCL, PT-TCL significantly increased CD69 expression in JURKAT cells, elevated the secretion of IL-2, IL-4, and TNF-β cytokines, and reduced lymphocyte apoptosis. Furthermore, PT-TCL activated TALL-104 cells and exhibited higher cytotoxicity against breast cancer cells *in vitro*. In summary, these findings demonstrate that PD-L1 nuclear translocation increases TCL immunoreactivity and promotes the antitumor efficacy of TCL-based immunotherapy. These results provide mechanistic insights supporting the optimization of TCL-based immunotherapeutic approaches for breast cancer.

KEYWORDS: breast cancer, nuclear translocation, programmed death-ligand 1, tumor cell lysate, immune activity

INTRODUCTION

Breast cancer remains one of the most prevalent malignant tumors among women worldwide [1, 2], with its incidence rate ranking highest in China [3, 4]. Despite advances in treatment, breast cancer continues to have a relatively high mortality rate, and current clinical interventions often yield suboptimal results [5, 6]. In recent years, antitumor immunotherapy has emerged as a promising strategy in the treatment of various malignancies, aiming to activate the host immune system and improve its ability to identify and eliminate tumor cells [7–9]. Among the various available immunotherapy approaches, immune checkpoint blockade targeting programmed cell death protein 1 (PD-1) and its ligand PD-L1 has demonstrated significant efficacy in treating various tumors and is now a major focus of tumor immunotherapy research [10–12].

The PD-1/PD-L1 signaling axis plays an essential role in tumor immune evasion [13]. Tumor cells can upregulate PD-L1 expression via multiple mechanisms, allowing PD-L1 to bind PD-1 receptors on the surface of T cells, inhibiting T cell-mediated cytotoxic activity, and facilitating immune escape, tumor growth, and metastasis [14]. When tumor cells undergo lysis, PD-L1 expressed by tumor cells is released along with various intracellular components into the tumor cell lysate (TCL).

TCL has recently gained significant attention due to its potential to elicit antitumor immune responses. Studies have found that the sensitization of immune cells with TCL can promote tumor-specific immune activity [15]. However, optimizing TCL-induced immune responses remains challenging, and current studies have mainly employed TCL prepared from wild-type tumor cells. TCL derived from mutant cells or cells treated with chemotherapy agents has been less explored, and their immunological characteristics and relevance to tumor progression are not well defined.

Emerging evidence indicates that the subcellular localization of PD-L1 can be altered in circulating tumor cells or breast cancer cells following exposure to chemotherapeutic agents such as doxorubicin [16, 17]. Studies have shown that nuclear-localized PD-L1 (nPD-L1) may increase the inflammatory response within the tumor microenvironment, facilitate neoantigen presentation, and activate multiple immune signaling pathways [18]. Since PD-L1 is detectable in TCL, the immunological impact of nPD-L1 may differ significantly from that of membrane-bound PD-L1, warranting further investigation.

To further investigate the role of nPD-L1 in TCL, doxorubicin was used in this study to induce PD-L1 nuclear translocation in breast cancer cells. TCL was then prepared from these treated cells (PT-TCL, containing nPD-L1) and untreated breast cancer cells (PN-TCL, containing non-nuclear PD-L1). These TCL preparations were applied to T lymphocytes to evaluate whether PT-TCL could increase T cell activation and promote stronger antitumor immune responses compared to PN-TCL.

This study aims to identify key molecules affecting the immunogenicity of TCL and elucidate the role of nPD-L1 in modulating TCL-mediated immune activa-

tion. The findings are expected to contribute to the mechanistic understanding of TCL-based immunotherapy and provide a theoretical foundation for improving immunotherapeutic strategies in breast cancer.

MATERIALS AND METHODS

Cell culture

MDA-MB-231, BT-474, and ZR-75-1 breast cancer cell lines were obtained from the National Collection of Authenticated Cell Cultures, Chinese Academy of Sciences. JURKAT cells were acquired from Guangzhou Cellcook Biotech Co., Ltd., Guangzhou, China, and TALL-104 cells were obtained from Shanghai Xuanya Biotechnology Co., Ltd., Shanghai, China. MDA-MB-231 cells were maintained in DMEM (Wisent Biotechnology Co., Ltd., Nanjing, China) supplemented with 10% fetal bovine serum (FBS; catalog number S711-001S; Lonsera Science SRL, Shanghai, China) and 100 U/ml penicillin-streptomycin (Beyotime Biotechnology Co., Ltd., Shanghai, China). BT-474, ZR-75-1, and JURKAT cells were cultured in RPMI-1640 (Wisent Biotechnology Co., Ltd.) medium supplemented with 10% FBS and 100 U/ml penicillin-streptomycin. All cells were cultured at 37 °C in a humidified atmosphere containing 5% CO_2, and cells in the logarithmic growth phase were used for experiments.

Preparation of tumor cell lysates (TCLs)

MDA-MB-231, BT-474, and ZR-75-1 cells were resuspended in phosphate-buffered saline (PBS; Biosharp Co., Ltd., Hefei, China) at a concentration of 1×10^7 cells/ml. Cell suspensions underwent 3–5 freeze-thaw cycles (−80 °C for 15 min and 37 °C for 5 min) to induce cell lysis. TCL formation was confirmed using Trypan blue staining under a light microscope.

Western blot analysis

Cytoplasmic, nuclear, and total proteins were extracted from MDA-MB-231, BT-474, and ZR-75-1 cells. Initially, cytoplasmic and nuclear proteins were extracted using a Nuclear Protein Extraction Kit (BestBio, BB-3102, Shanghai, China). Cells were washed, trypsinized, and $5–10\times10^6$ cells were collected. Each 20 µl volume of cell precipitation (about 20 mg, 2×10^6 cells) was added with 200–300 µl cold extract solution A, mixed with high-speed vortex oscillation or blow mixing, and oscillated at 2–8 °C for 10–30 min. Then centrifuge at 4 °C, 2,000×g, for 5 min. The supernatant is inhaled into another pre-cooled clean centrifuge tube to obtain cytoplasmic protein. Add 80–200 µl of cold extract B to the precipitate and swirl at high speed for 15 s. Oscillate at 2–8 °C for 30–40 min. Centrifuge for 10 min at 4 °C, 12,000×g. The supernatant is sucked into another pre-cooled clean centrifuge tube to obtain the nuclear protein. The method for total cellular protein extraction was as follows: According to the number of cells, 100 µl of prepared cell lysis buffer containing PMSF was added per 1×10^6 cells. The cells were thoroughly mixed by pipetting and incubated with shaking at 2–8 °C for 10–30 min until no obvious precipitate remained. The centrifuge was pre-cooled to 4 °C, and the cell lysates were further centrifuged at 12,000 rpm for 10 min at 4 °C. The supernatant was transferred to another pre-cooled clean centrifuge tube to obtain the total protein fraction. Proteins were separated by SDS-PAGE and transferred to PVDF membranes. Membranes were incubated at 4 °C overnight with primary antibodies from rabbit: PD-L1/CD274 mAb (A19135), PD-1/CD-279 pAb (A11973), HRP-conjugated GAPDH mAb (AC054), and HDAC2 mAb (A19626) from ABClonal Biotechnology Co., Ltd., Hubei, China. After washing, membranes were incubated with HRP-conjugated goat anti-rabbit IgG secondary antibody (Beyotime Biotechnology Co., Ltd.) at room temperature. Protein expression levels were visualized using chemiluminescence imaging and analyzed using ImageJ software.

Flow cytometric analysis

PBS, PN-TCL, and PT-TCL were applied to JURKAT cells at the tumor cell:T cell ratios of 0.25:1, 0.5:1, 1:1, 2:1, and 3:1 for 24, 48, and 72 h. After treatment, JURKAT cells were collected, washed twice with pre-cooled PBS (2,000 rpm, 5 min, 4 °C), and resuspended in 500 µl staining buffer. Cells were stained with propidium iodide (PI) and Annexin V-FITC (KeyGen BioTECH Co., Ltd., Nanjing, China) at 4 °C for 15 min in the dark, followed by apoptosis analysis using a Beckman flow cytometer within 1 h. Data were analyzed using FlowJo software (v10.8, BD Biosciences, Ashland, USA). Debris and doublets were excluded based on FSC-A/SSC-A and FSC-H/FSC-A gating. Annexin V−/PI− cells were defined as viable, Annexin V+/PI− as early apoptotic, Annexin V+/PI+ as late apoptotic, and Annexin V−/PI+ as necrotic. The total apoptotic rate was calculated as the sum of early and late apoptotic populations.

To assess the effect of different TCL on T cell activation, JURKAT cells treated with PBS, PN-TCL, or PT-TCL were stained with PE-conjugated anti-CD69 antibody (BioLegend Inc., San Diego, CA, USA) and analyzed using flow cytometry.

Immunofluorescence staining

MDA-MB-231, BT-474, and ZR-75-1 cells were seeded on coverslips in culture plates and cultured overnight at 37 °C in a 5% CO_2 incubator. After replacing the medium with a fresh culture medium, cells were treated with various concentrations of doxorubicin for 72 h. Then, the old medium was discarded, and cells were fixed at room temperature with a fixative solution for 15–30 min, then permeabilized using 1–2 ml immunostaining permeabilization buffer for 20 min at room temperature. Blocking was then performed

with 200 µl goat serum blocking buffer for 30 min at room temperature. Cells were incubated sequentially with primary antibodies and fluorescently labeled secondary antibodies for 1 h each at room temperature in the dark. Nuclear staining was conducted using 500 µl of 1 × DAPI staining solution for 5–10 min at room temperature. Finally, coverslips were mounted with anti-fade reagent and observed under a fluorescence microscope.

Enzyme-linked immunosorbent assay (ELISA)

JURKAT cells (2.5×10^5) were seeded into 12-well plates. After the stabilization of JURKAT cells, equal doses of PN-TCL and PT-TCL derived from the three breast cancer cell lines were added to the wells. A PBS-treated group served as the control. After 48 h of incubation, supernatants were collected. IL-2, IL-4, and TNF-β concentrations were measured using ELISA kits (ABClonal Biotechnology Co., Ltd.) according to the manufacturer's instructions. Finally, 100 µl of stop solution was added to each well to terminate the reaction. Optical density (OD value) was measured at 450 nm within 10 min using an EPOCH microplate spectrophotometer (BioTek Instruments, Inc., Winooski, VT, USA).

Cell proliferation and cytotoxicity assay

TCLs derived from untreated and doxorubicin-treated MDA-MB-231, BT-474, and ZR-75-1 cells were applied to TALL-104 cells and incubated for 48 h at 37 °C in a 5% CO_2 incubator. Activated TALL-104 cells were collected and counted. For the cytotoxicity assay, breast cancer cells were used as target cells and TALL-104 cells as effector cells. Effector and target cells were co-cultured at effector-to-target (E:T) ratios of 5:1, 10:1, 20:1, and 40:1 for 24 h. Wells containing only target cells served as controls. After 24 h, CCK-8 reagent (KeyGen BioTECH Co., Ltd.) was added, and optical density at 450 nm was measured 1–4 h later using a microplate reader.

Quantitative real-time PCR (qPCR)

Total RNA was extracted by adding 1 ml Trizol reagent (Life Technologies Corporation, Carlsbad, CA, USA) to the cell samples, followed by the addition of 0.2 ml chloroform. Samples were mixed and incubated at room temperature for 2–3 min, then centrifuged (12,000×g) for 15 min. The aqueous phase was collected, mixed with an equal volume of 70% ethanol, and transferred to an RNA spin column. After standing for 2 min, columns were centrifuged at 12,000×g for 3 min. The flow-through was discarded, and columns were washed 1–2 times. RNA was eluted with 30–50 µl RNase-free DEPC-treated water and incubated at room temperature for 5 min before final centrifugation. RNA was reverse-transcribed into cDNA and qPCR was performed using the resulting cDNA templates (TAKARA BIO INC., Kusatsu, Shiga Prefecture, Japan). The PCR conditions were as follows: preincubation at 95 °C for 30 s, then denaturation at 95 °C for 5 s underwent 40 cycles and extension at 60 °C for 30 s.

Statistical analysis

All data were expressed as mean ± standard deviation (SD), and each experiment was repeated in independent biological triplicate. Data were initially analyzed using one-way ANOVA. For comparisons between two groups, the t-test was applied if variances were equal; otherwise, the rank-sum test was used. For multiple group comparisons, one-way analysis of variance (ANOVA) followed by Tukey's post-hoc test was conducted to correct for multiple testing. A p value less than 0.05 was considered statistically significant. All statistical analyses were performed using GraphPad Prism version 8.0 for Windows.

RESULTS

Expression and intracellular location of PD-L1 in MDA-MB-231, BT-474 and ZR-75-1 cells

Three breast cancer cell lines (MDA-MB-231, BT-474, and ZR-75-1) were cultured under optimal conditions to 70–80% confluency and lysed for protein extraction from the treated cells to evaluate the expression of PD-L1. Western blot results revealed detectable PD-L1 expression in all three cell lines. However, PD-L1 levels were significantly higher in MDA-MB-231 cells and BT-474 cells compared to ZR-75-1 cells ($p < 0.01$; Fig. 1A). In parallel, PD-1 expression in JURKAT cells was confirmed by the same method as above, showing positive expression (Fig. 1B). To assess whether doxorubicin affects PD-L1 localization in breast cancer cell lines MDA-MB-231, BT-474, and ZR-75-1, immunofluorescence staining was performed following treatment with various concentrations of doxorubicin (0 µg/ml, 0.4 µg/ml, and 0.8 µg/ml) for 72 h. In untreated MDA-MB-231 cells, PD-L1 was mainly localized to the cell membrane and cytoplasm, with only minimal nuclear expression. After treatment with 0.4 µg/ml doxorubicin, nuclear accumulation of PD-L1 significantly increased (Fig. 1C). Similar changes were observed in BT-474 and ZR-75-1 breast cancer cells after treatment with 0.4 µg/ml doxorubicin (Fig. 1D), although the degree of nuclear PD-L1 translocation was less significant than in MDA-MB-231 cells (Fig. 1C–E). These results indicate that doxorubicin induces nuclear translocation of PD-L1 in breast cancer cells.

Effects of doxorubicin at different doses on PD-L1 expression

To further validate the redistribution of PD-L1 following doxorubicin exposure, Western blot analysis was conducted using total, cytoplasmic, and nuclear protein extracts from MDA-MB-231, BT-474, and ZR-75-1 cells treated with 0, 0.4, or 1.6 µg/ml doxorubicin for 72 h. Western blot analysis revealed that

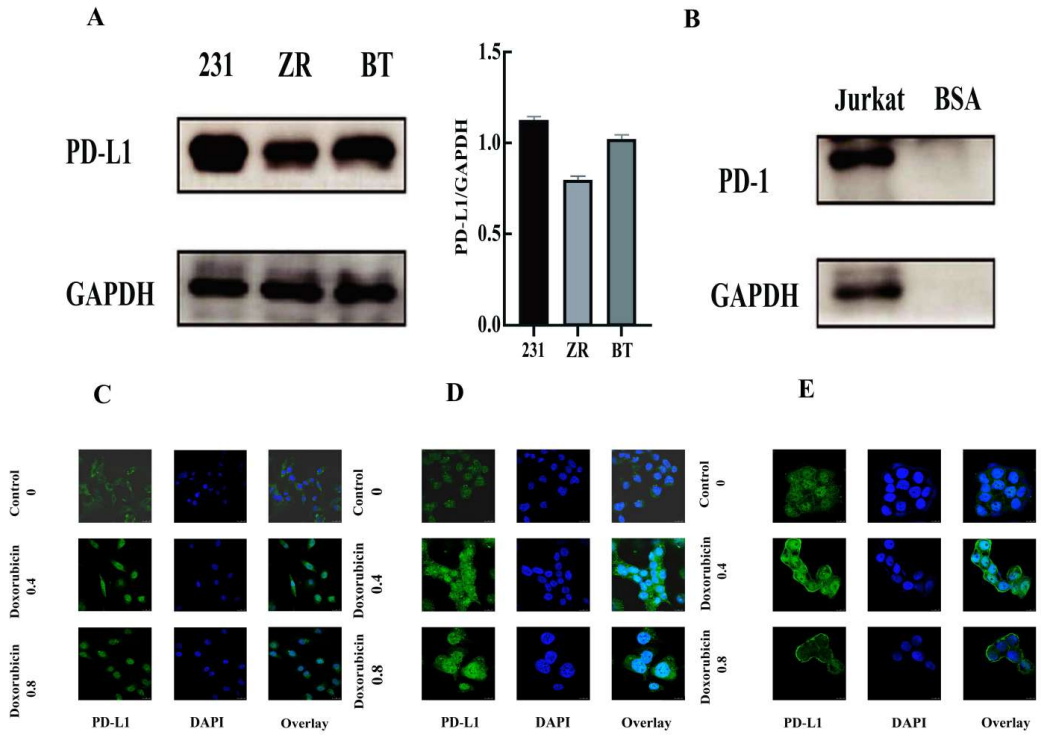

Fig. 1 Expression of PD-L1 and PD-1 proteins in different cell lines and intracellular location of PD-L1 in three breast cancer cells treated by doxorubicin. (A) Expression of PD-L1 and internal reference GAPDH in MDA-MB-231, BT-474, and ZR-75-1 breast cancer cell lines. (B) PD-1 expression in JURKAT cells. *** $p < 0.001$; ** $p < 0.01$; * $p < 0.05$. (C–E) Effect of doxorubicin on the subcellular distribution of PD-L1 in breast cancer cells. Immunofluorescence images of MDA-MB-231 cells, BT-474 cells, and ZR-75-1cells. The left column represents the distribution of PD-L1 (green fluorescence), the middle column shows nuclei stained by DAPI (blue fluorescence), and the right column is the overlay image combining PD-L1 and DAPI signals. The rows from top to bottom correspond to the control group (no doxorubicin) and treatment groups with 0.4 and 0.8 µg/ml doxorubicin, respectively. $n = 3$.

compared with untreated controls, cells treated with 0.4 µg/ml doxorubicin showed decreased cytoplasmic PD-L1 levels alongside significantly increased nuclear PD-L1 expression ($p < 0.01$; Fig. 2A–C). Moreover, expression of HDAC2, a nuclear protein, was significantly upregulated following doxorubicin treatment, particularly at 0.4 µg/ml, in all three breast cancer cell lines. Among them, MDA-MB-231 cells demonstrated the most significant increase in nuclear HDAC2 levels compared to BT-474 and ZR-75-1 (Fig. 2A–C).

Dose- and time-dependent induction of apoptosis by PN-TCL in JURKAT cells

To evaluate the pro-apoptotic effects of TCL derived from breast cancer cells on JURKAT cells, various doses of TCL and incubation times were investigated. Flow cytometric analysis demonstrated that apoptosis in JURKAT cells increased in a dose-dependent manner at 24, 48, and 72 h, with higher TCL-to-JURKAT cell ratios resulting in a significant increase in apoptosis ($p < 0.01$). At the 48 h time point, TCL from MDA-MB-231 and BT-474 induced the highest apoptosis rate at a 2:1 cell ratio (tumor cells: JURKAT cells) (Fig. 3A,B). At the 48 h time point, ZR-75-1-derived TCL induced maximal JURKAT apoptosis at a 3:1 ratio (Fig. 3C). Based on these results, optimal conditions for subsequent experiments were established as follows: a 2:1 ratio for MDA-MB-231- and BT-474-derived TCL, a 3:1 ratio for ZR-75-1-derived TCL, and a treatment duration of 48 h for all experimental groups.

Effect of PT-TCL on apoptosis of JURKAT cells

To assess whether nuclear translocation of PD-L1 in tumor cells alters their immunogenic potential, JURKAT cells were treated with PT-TCL (TCL containing nuclear-translocated PD-L1) or PN-TCL (from normal breast cancer cells). Apoptosis was quantified via flow cytometry. For TCLs derived from MDA-MB-231 cells, apoptosis rates of JURKAT cells in the PBS control, PN-TCL, and PT-TCL groups were 3.8%, 13%, and 7.2%, respectively ($p < 0.001$; Fig. 4A). A similar pattern was observed for BT-474-derived TCL, with respective apoptosis rates of 4.3%, 9.6%, and 4.1% ($p < 0.001$; Fig. 4B). ZR-75-1-derived TCL also induced apoptosis

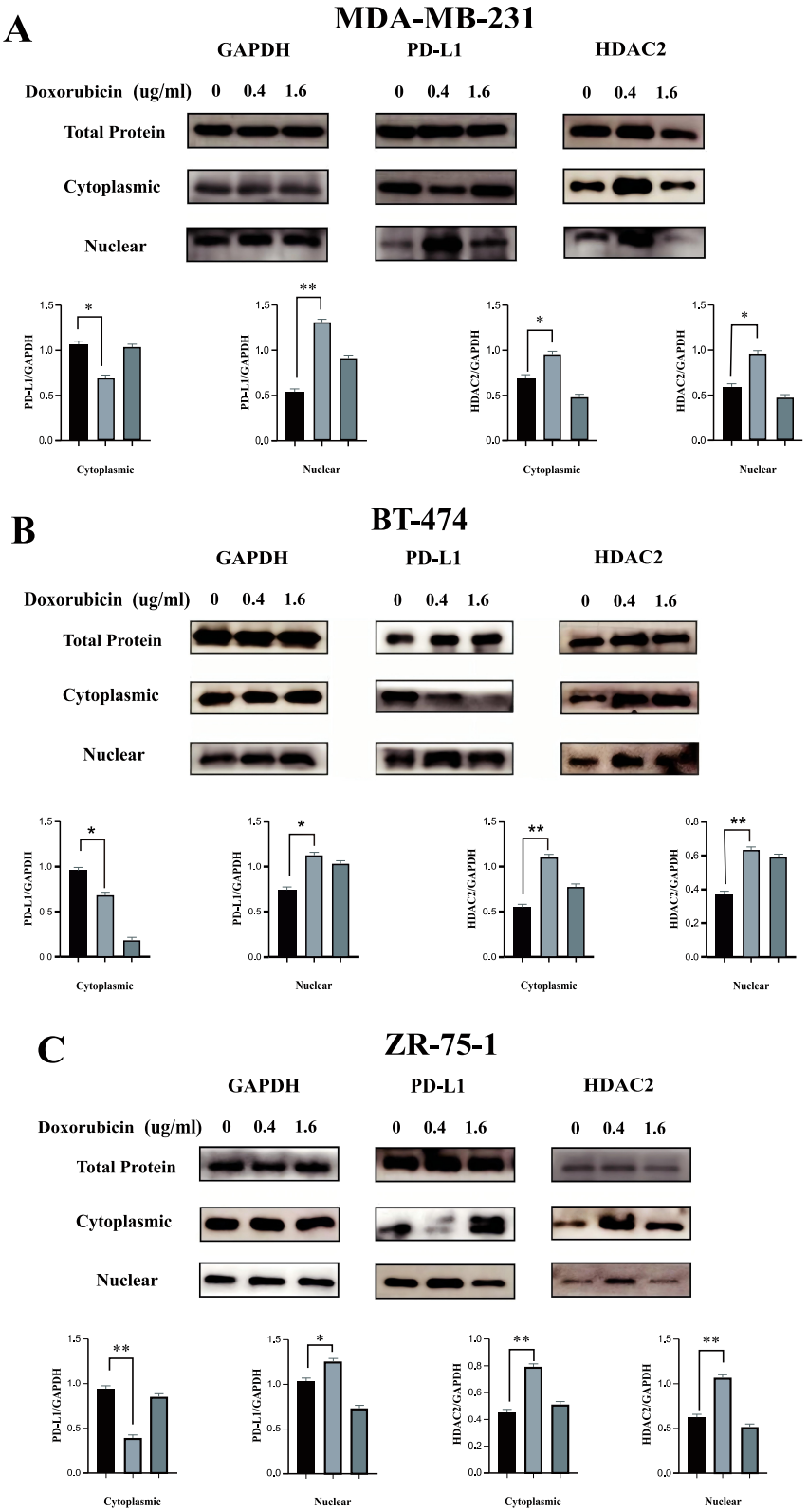

Fig. 2 Western blot analysis of PD-L1 and HDAC2 protein expression following doxorubicin treatment. (A–C) Expression levels of GAPDH, PD-L1, and HDAC2 in MDA-MB-231, BT-474, and ZR-75-1 cells treated with 0, 0.4, and 1.6 µg/ml doxorubicin. $n = 3$. *** $p < 0.001$, ** $p < 0.01$, * $p < 0.05$.

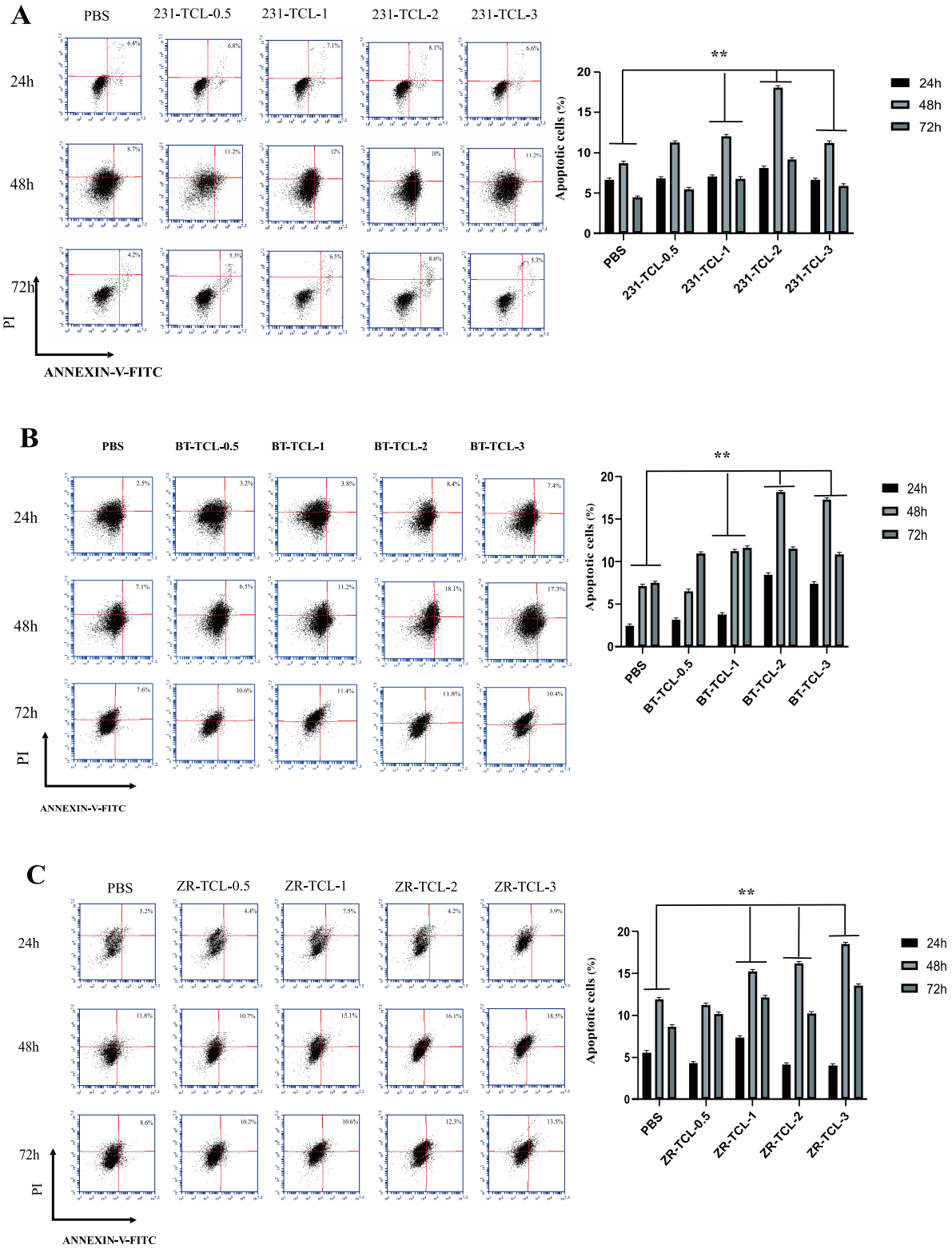

Fig. 3 Apoptosis of JURKAT cells induced by PN-TCL at different ratios and time points. (A–C) Flow cytometric analysis of apoptosis using Annexin V-FITC and Propidium iodide (PI) staining after treatment with PBS or MDA-MB-231-TCL, BT-474-TCL, and ZR-75-1-TCL at ratios of 0.5:1, 1:1, 2:1, and 3:1 for 24, 48, and 72 h. $n = 3$. *** $p < 0.001$, ** $p < 0.01$, * $p < 0.05$.

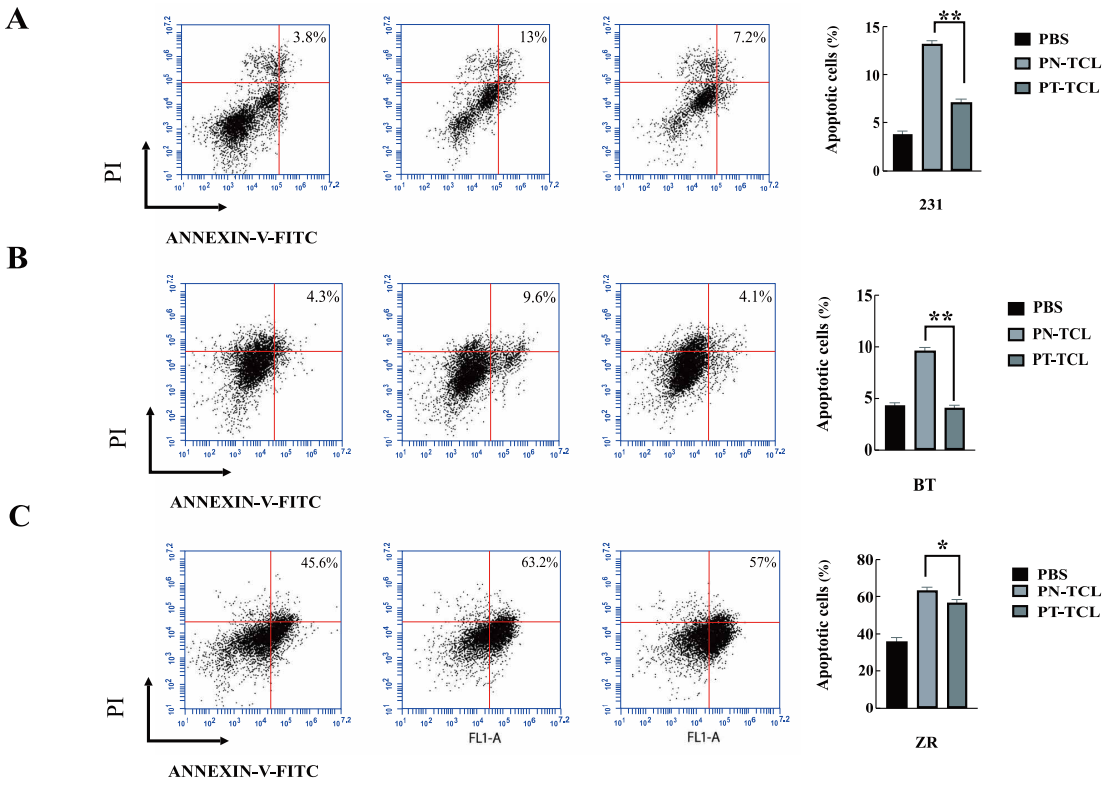

Fig. 4 Apoptosis of JURKAT cells induced by PN-TCL and PT-TCL. (A–C) Flow cytometric dot plots showing Annexin V-FITC/PI-stained JURKAT cells treated with PBS, PN-TCL, and PT-TCL from MDA-MB-231, BT-474, or ZR-75-1 for 48 h. $n = 3$. *** $p < 0.001$, ** $p < 0.01$, * $p < 0.05$.

at 45.6%, 63.2%, and 57% in the three groups, respectively ($p < 0.01$; Fig. 4C). These findings suggest that PT-TCL exhibits a reduced capacity to induce apoptosis in JURKAT cells compared with PN-TCL.

Effect of PT-TCL on the activation of JURKAT cells

To determine the activation status of JURKAT cells induced by different TCL preparations, the surface expression of the activation marker CD69 for JURKAT cells was analyzed by flow cytometry. When exposed to TCL from MDA-MB-231 cells, the proportions of CD69-positive cells in the PBS control, PN-TCL, and PT-TCL groups were 14.1%, 44.2%, and 55.9%, respectively. CD69 expression was significantly elevated in the PT-TCL group compared to other groups ($p < 0.0001$; Fig. 5A). Similarly, JURKAT cells treated with BT-474-derived PT-TCL showed higher CD69 expression (85.4%) compared with the PBS control (33%) and PN-TCL groups (76.6%) ($p < 0.001$; Fig. 5B). For ZR-75-1-derived TCL, CD69 expression was 23%, 74.1%, and 79.9% in the PBS, PN-TCL, and PT-TCL groups, respectively ($p < 0.01$; Fig. 5C). These results indicate that PT-TCL treatment induces higher activation of JURKAT cells, as shown by upregulated CD69 expression, despite reduced apoptotic induction.

The effect of PT-TCL on the secretion of cytokines by JURKAT cells

To further explore the immunomodulatory effects of PT-TCL on JURKAT cell activation, the secretion levels of IL-2, IL-4, and TNF-β cytokines were quantified following 48 h treatments with PBS, PN-TCL, and PT-TCL. ELISA analysis demonstrated that JURKAT cells treated with PT-TCL derived from all three breast cancer cell lines exhibited significantly increased secretion of IL-2, IL-4, and TNF-β compared to the PBS and PN-TCL groups ($p < 0.01$). Among the three sources, PT-TCL from BT-474 induced the highest secretion levels of all three cytokines. PT-TCL from ZR-75-1 stimulated higher secretion of IL-2 and IL-4 compared to MDA-MB-231-derived PT-TCL, whereas MDA-MB-231 PT-TCL elicited stronger TNF-β secretion than ZR-75-1 ($p < 0.01$; Fig. 6A–C). These findings indicate that PT-TCL promotes JURKAT cell activation and production of cytokines IL-2, IL-4, and TNF-β more effectively than PN-TCL.

Cytotoxicity of TALL-104 cells against breast cancer cells

Activated TALL-104 cells, which are cytotoxic CD8+ T lymphocytes, exhibit potent tumoricidal activity

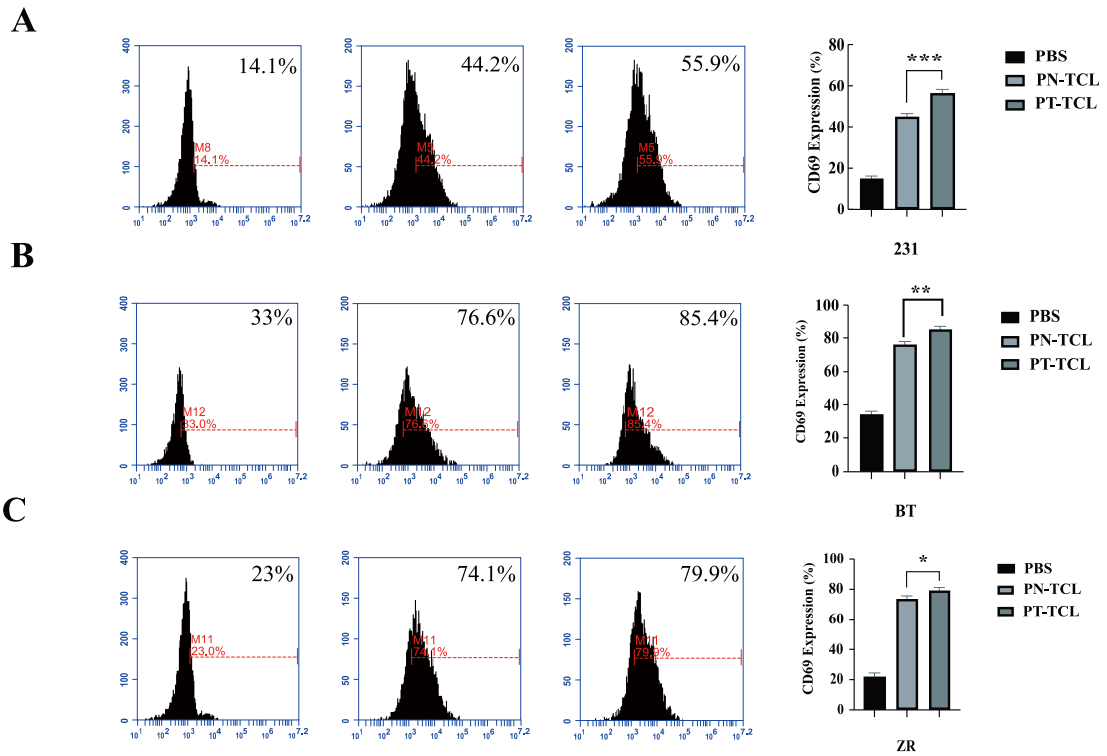

Fig. 5 Flow cytometric analysis of CD69 expression in JURKAT cells treated with PN-TCL and PT-TCL. (A–C) Cell activation results of JURKAT cells after being treated with different TCLs from MDA-MB-231, BT-474, or ZR-75-1. Flow cytometric histograms showing the CD69 expression in JURKAT cells treated with PBS, PN-TCL, and PT-TCL after 48 h, respectively. $n = 3$. *** $p < 0.001$, ** $p < 0.01$, * $p < 0.05$.

against tumor cells. To evaluate the cytolytic function of activated TALL-104 cells against breast cancer cells, TCLs from MDA-MB-231, BT-474, and ZR-75-1 were used to activate TALL-104 cells for 48 h. Effector cells were then co-cultured with target tumor cells at effector-to-target (E:T) ratios of 5:1, 10:1, 20:1, and 40:1 for 24 h. Cell viability was assessed using the CCK-8 assay. PT-TCL-activated TALL-104 cells demonstrated significantly higher cytotoxicity than those activated with PN-TCL or PBS. For MDA-MB-231 target cells, the cytotoxic rates at an E:T ratio of 40:1 in PBS, PN-TCL, and PT-TCL groups were 47.4%, 53.5%, and 89.9%, respectively ($p < 0.001$; Fig. 7A). For BT-474, these values were 68.6%, 78.8% and 91.7% ($p < 0.01$; Fig. 7B), and for ZR-75-1, 42.3%, 52.5%, and 76.3%, respectively ($p < 0.01$; Fig. 7C). In all tested conditions, the PT-TCL group showed the highest cytotoxicity efficacy.

Establishment of PD-L1 knockdown in MDA-MB-231 cell line and effects of TCL on T lymphocyte apoptosis

To investigate whether nPD-L1 in TCL is responsible for its reduced pro-apoptotic effect on T lymphocytes, PD-L1 expression was silenced in MDA-MB-231 cells *via* siRNA-mediated knockdown. Three siRNAs (siPD-L1-1/2/3) were transfected to generate PD-L1-deficient cells, which were used to prepare PK-TCL (TCL from PD-L1-deficient cells). The effects of PN-TCL, PT-TCL, and PK-TCL on JURKAT cell apoptosis were analyzed by flow cytometry. qPCR confirmed that all three siRNAs significantly inhibited PD-L1 mRNA expression compared with the siCtrl group, with knockdown efficiencies of 62%, 23%, and 17%, respectively ($p < 0.01$; Fig. 8A). The siPD-L1-1 displayed the highest interference efficiency and was selected for subsequent experiments. Western blot analysis confirmed the reduction in PD-L1 protein expression in siPD-L1-1, siPD-L1-2, and siPD-L1-3 cells compared with the control group (Fig. 8B). Apoptosis rates (early + late) in JURKAT cells treated with PK-TCL, PN-TCL, and PT-TCL were 26.0%, 32.3% and 27.9%, respectively (Fig. 8C). Statistical analysis revealed a significant difference between PK-TCL and PN-TCL groups ($p < 0.01$), whereas no significant difference was observed between PK-TCL and PT-TCL groups ($p > 0.05$). The nuclear translocation of PD-L1 may reduce its surface availability and, therefore, impair PD-1 binding, reducing its pro-apoptotic capacity. To investigate this effect, we used doxorubicin to treat MDA-MB-231 cells at 0.2 µg/ml or 0.4 µg/ml concentrations. TCL was then prepared from these cells and applied to H9 cells at

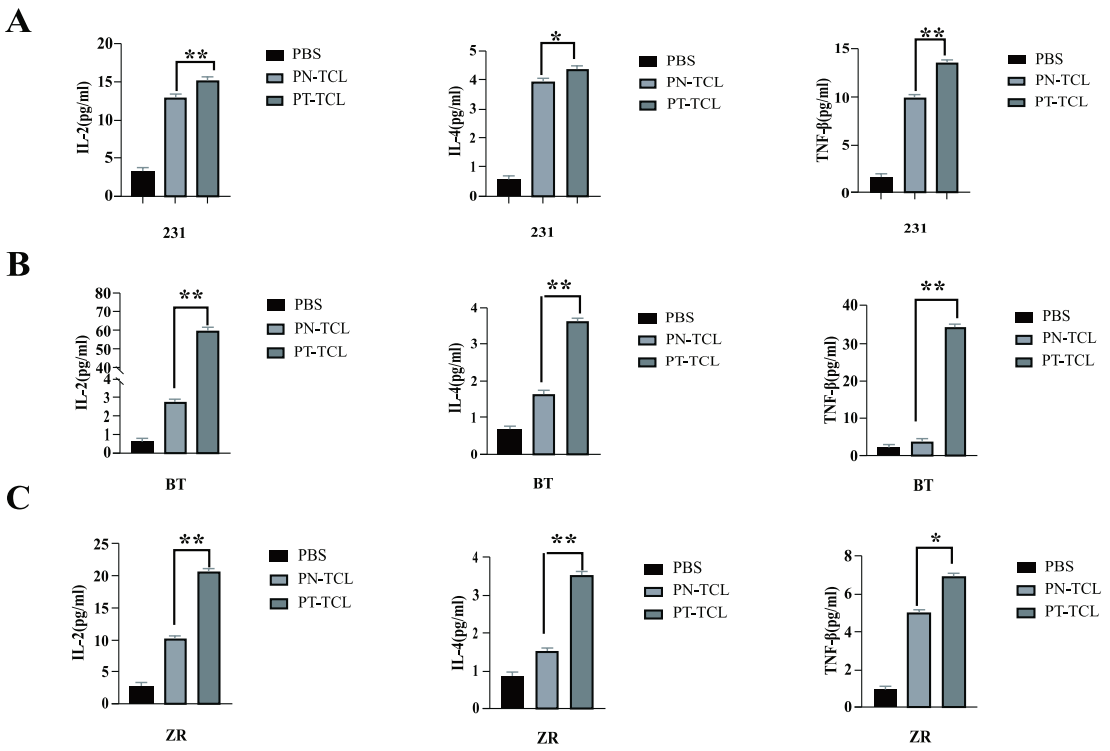

Fig. 6 Cytokine secretion by JURKAT cells in response to PN-TCL and PT-TCL. (A–C) ELISA results showing concentrations of IL-2, IL-4, and TNF-β in the supernatants of JURKAT cells treated with PBS, PN-TCL, or PT-TCL from MDA-MB-231, BT-474, or ZR-75-1. Each set of histograms shows the concentration of IL-2, IL-4, and TNF-β cytokines (from left to right) in the supernatant of JURKAT cells treated with PBS, PN-TCL, and PT-TCL. $n = 3$. *** $p < 0.001$, ** $p < 0.01$, * $p < 0.05$.

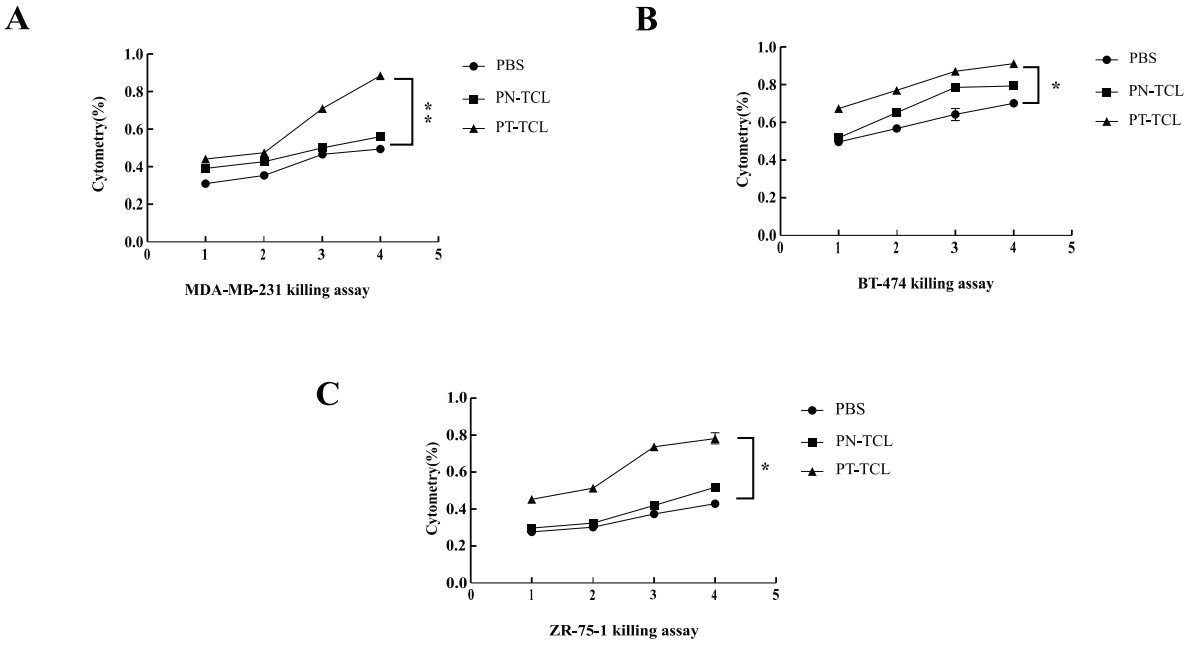

Fig. 7 Cytotoxicity of TALL-104 cells against breast cancer cell lines. (A–C) Cell viability assays (CCK-8) of MDA-MB-231, BT-474, and ZR-75-1 cells co-cultured with TALL-104 cells at effector-to-target (E:T) ratios of 5:1, 10:1, 20:1, and 40:1 for 24 h [effector cell:tall-104; target cells:the three breast cancer cells]. $n = 3$. *** $p < 0.001$, ** $p < 0.01$, * $p < 0.05$.

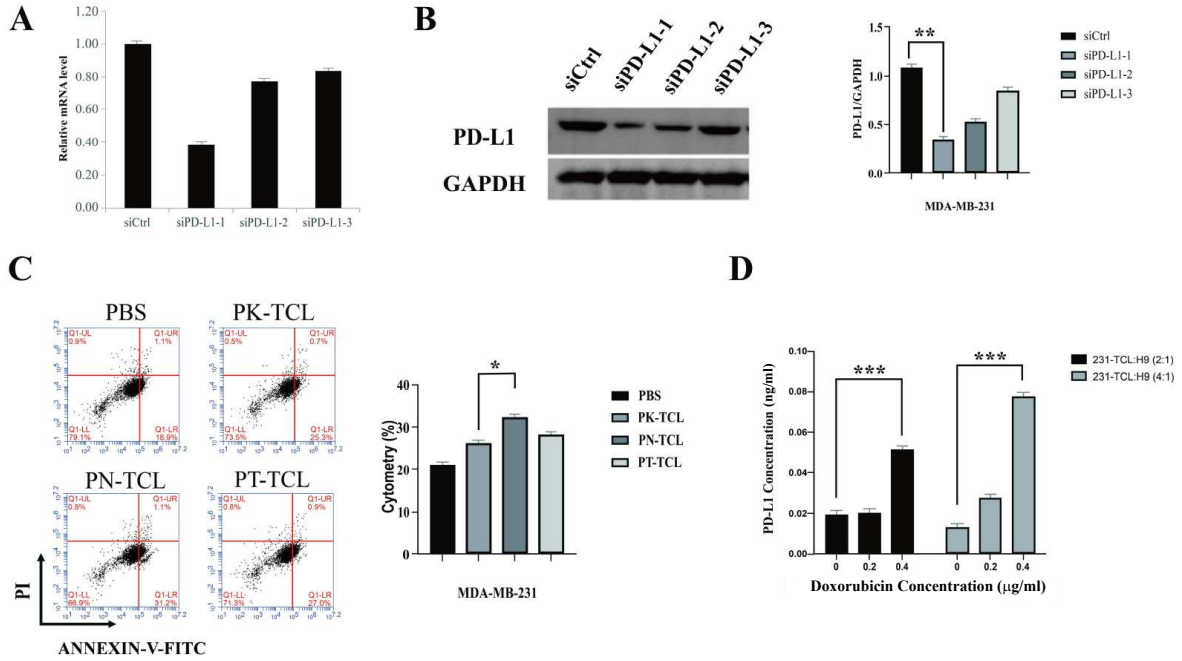

Fig. 8 Effect of PK-TCL on JURKAT cell apoptosis. (A) q-PCR analysis of PD-L1 mRNA expression in MDA-MB-231 cells transfected with three independent siRNAs (siPD-L1-1/2/3) or control siRNA (siCtrl). (B) PD-L1 protein levels in siRNA-transfected cells. (C) The apoptosis rate of JURKAT treated with PK-TCL, PN-TCL, or PT-TCL. (D) ELISA detection of PD-L1 in the culture medium supernatants of H9 cells treated with TCL derived from MDA-MB-231 cells induced with 0, 0.2, or 0.4 μg/ml doxorubicin for 48 h. H9 cells were treated at tumor cell-to-H9 cell ratios of 2:1 and 4:1. $n = 3$. *** $p < 0.001$, ** $p < 0.01$, * $p < 0.05$.

tumor cell-to-H9 cell ratios of 2:1 and 4:1 for 48 h. PD-L1 concentrations in the culture supernatants were quantified *via* ELISA. PT-TCL prepared from MDA-MB-231 treated with 0.4 μg/ml doxorubicin consistently exhibited high PD-L1 levels, regardless of the cell ratio of 2:1 or 4:1 ($p < 0.01$; Fig. 8D). These results suggest that nPD-L1 demonstrates reduced capacity to bind PD-1 on the surface of T lymphocytes, thus changing its immunomodulatory function.

DISCUSSION

PD-L1, a ligand expressed on tumor cells [19], binds to PD-1 receptors on T lymphocytes, activating inhibitory signaling pathways that facilitate immune escape and tumor progression [16, 20]. In solid tumors, particularly breast cancer, PD-L1 is highly expressed in tumor cells and tumor-infiltrating immune cells [21–23]. Genomic amplification of *CD274*, the gene encoding PD-L1, is frequently observed in breast cancer and is strongly associated with poor clinical prognosis [24–26].

The subcellular distribution of PD-L1 varies across tumor specimens, where PD-L1 is primarily localized to the plasma membrane and cytoplasm, though nuclear expression has also been reported [27]. Positive nPD-L1 expression has been identified in surgically resected samples of renal cell carcinoma, lung cancer, and hepatocellular carcinoma [28, 29]. In human breast cancer, nPD-L1 switches TNF-β-induced apotheosis proptosis in tumor cells [30]. Similarly, in lung cancers, induction of nuclear PD-L1 translocation inhibits tumorigenesis and enhances antitumor immunity [31]. In breast cancer, doxorubicin has been reported to increase the expression of nPD-L1 levels via AKT phosphorylation [32].

In this study, doxorubicin was used to induce PD-L1 nuclear translocation in breast cancer cells, allowing the preparation of TCL containing nPD-L1 (PT-TCL). The objective was to investigate its immunological effects and whether such TCL preparations could display improved immunoactivity, potentially supporting the development of novel cancer immunotherapeutic strategies.

PD-L1 expression in three breast cancer cell lines, MDA-MB-231, BT-474, and ZR-75-1, was first assessed and then investigated whether JURKAT immune cells expressed PD-1. Western blotting revealed that PD-L1 expression was highest in MDA-MB-231 cells, followed by BT-474 cells, and was lowest in ZR-75-1 cells. These findings suggest differential PD-L1 expression among breast cancer cell types, which may affect the immunoregulatory capacity of TCL prepared from these breast cancer cells. Moreover, PD-1 expression in JURKAT cells confirmed the presence of the molecular machinery necessary to initiate immune checkpoint signaling.

To determine the optimal TCL-to-immune cell ratio and incubation time, JURKAT cells apoptosis induced by the three breast cancer cell lines was analyzed using flow cytometry. Maximum apoptosis was observed at a 2:1 TCL-to-JURKAT ratio after 48 h for both MDA-MB-231-TCL and BT-474-TCL, whereas ZR-75-1-TCL required a 3:1 ratio to achieve a comparable effect. Based on Western blot analysis of PD-L1 molecular content in the TCLs, it was hypothesized that the capacity of TCLs to induce apoptosis in JURKAT cells was closely associated with their PD-L1 content. These results suggest that PD-L1 is a key effector molecule mediating TCL-induced apoptosis in JURKAT immune cells.

To investigate the functional impact of nPD-L1 on TCL immunogenicity, MDA-MB-231, BT-474, and ZR-75-1 cells were treated with 0.4 μg/ml doxorubicin to induce PD-L1 nuclear translocation. Immunofluorescence microscopy confirmed the accumulation of nPD-L1 in all three breast cancer cell lines following treatment. Protein immunoblotting demonstrated increased nPD-L1 expression in all three cell types post-treatment, with the most significant upregulation observed in MDA-MB-231 cells. The upregulation in BT-474 was more apparent than in ZR-75-1. PD-L1 acetylation at lysine 263 in the cytoplasmic domain is catalyzed by the p300 acetyltransferase, and this modification is reversed by HDAC2. HDAC2-mediated deacetylation facilitates PD-L1 nuclear translocation, whereas HDAC2 inhibition or deficiency increases acetylation and reduces nuclear localization [18, 34]. In this study, HDAC2 expression was elevated in all three breast cancer cell lines after treatment with 0.4 μg/ml doxorubicin, supporting the role of HDAC2-catalyzed deacetylation in promoting PD-L1 nuclear translocation.

To assess the immunological consequences of nPD-L1 in TCL, JURKAT cells were treated with PN-TCL and PT-TCL. Flow cytometric analysis revealed that PT-TCL significantly reduced apoptosis and increased expression of the CD69 activation marker in JURKAT cells compared with PN-TCL. CD69 is a well-established marker of early T-cell activation [35–37]; thus, its increased expression indicates improved immunostimulatory capacity. These results suggest that PT-TCL attenuates T-cell apoptosis and improves activation potential relative to PN-TCL. Among the cell lines, PT-TCL derived from MDA-MB-231 and BT-474 displayed stronger effects in reducing apoptosis and increasing CD69 expression than PT-TCL from ZR-75-1, indicating that the immunomodulatory capacities of TCL derived from different cell lines are variable.

Cytokine profiling further supported these observations. After 48 h of co-culture with PT-TCL from the three breast cancer cell lines, IL-2, IL-4, and TNF-β levels in JURKAT culture supernatants were significantly elevated compared with the PN-TCL groups. Among these, TNF-β secretion particularly increased in the MDA-MB-231 group, while IL-2 elevation was more significant in BT-474 and ZR-75-1 groups. IL-2 is known to activate macrophages and cytotoxic T lymphocytes [38], induce CD4+ T-cell differentiation into Th1 cells, and promote cellular immunity [39]. IL-4, primarily secreted by Th2 cells, supports humoral immune responses [40]. TNF-β, produced by activated T and B lymphocytes, binds to tumor cell receptors and activates apoptotic signaling, therefore inducing tumor cell death and inhibiting tumor progression. These findings suggest that PT-TCL improves antitumor immune responses by increasing cytokine secretion [41, 42]. To further evaluate antitumor efficacy, PT-TCL and PN-TCL were applied to TALL-104 cells, a cytotoxic T-cell line capable of destroying tumor cells both *in vivo* and *in vitro*. The activated TALL-104 cells were then co-cultured with breast cancer cells. The results showed that T lymphocytes activated by PT-TCL exhibited increased cytotoxicity against all three breast cancer cell lines. Among them, PT-TCL from MDA-MB-231 was the most effective, followed by BT-474 and ZR-75-1. These results, alongside previous Western blot data, suggest that the better cytotoxicity observed with MDA-MB-231-derived PT-TCL is likely due to its higher nPD-L1 content.

It has been reported that, in addition to promoting PD-L1 nuclear translocation, doxorubicin treatment upregulates the expression of several other proteins in breast cancer cells [43]. Therefore, in the context of three distinct breast cancer cell lines showing variable antitumor immunocompetence of TCL, it is necessary to consider whether changes in TCL components beyond nPD-L1 contribute to immune cell modulation. To determine whether the immunomodulatory effects of PT-TCL are specifically mediated by nPD-L1, a PD-L1 knockdown MDA-MB-231 cell line was generated, and PD-L1 knockdown TCL (PK-TCL) was prepared. JURKAT cells were treated with PK-TCL, PT-TCL, and PN-TCL, and apoptosis was then analyzed. The results indicated that apoptosis in JURKAT cells was significantly reduced following PK-TCL treatment compared with PN-TCL. Similarly, apoptosis in the PT-TCL group was significantly reduced compared with PN-TCL. However, no significant difference in apoptosis was observed between the PK-TCL and PT-TCL groups. These findings suggest that both PD-L1 knockdown and PD-L1 nuclear translocation impair TCL-induced apoptosis in T lymphocytes. Thus, the observed immunological effects are primarily due to changes in PD-L1 status rather than alterations in other TCL components induced by doxorubicin treatment.

To further evaluate this mechanism, PT-TCL and PN-TCL derived from MDA-MB-231 cells were applied to H9 cells. After 48 h, the concentration of PD-L1 in the culture supernatant was measured by ELISA. The results showed that the PD-L1 concentration in the PT-TCL group was significantly higher than that in the PN-TCL group. This may be due to conformational changes

in PD-L1 following nuclear translocation, which may reduce its binding affinity to PD-1 on the surface of lymphocytes. As a result, PD-L1 remains unbound and accumulates in the supernatant, thus decreasing lymphocyte apoptosis and contributing to enhanced antitumor immune activity in the PT-TCL group. This study has limitations. First, the reliance on immortalized T-cell lines may not fully mirror primary human T-cell biology. Second, the restricted cytokine types and the observed increase in IL-4 call for a more nuanced interpretation of the immune response state and suggest the need for broader profiling in future work.

CONCLUSION

In conclusion, nuclear translocation of PD-L1 in TCL significantly improves immune cell activation and elicits stronger anti-breast cancer immune responses. These findings indicate that strategic change of TCL components, particularly by manipulating the location of PD-L1 inside the cell, can improve its immunostimulatory ability. Given that this study is exclusively *in vitro*, our findings may offer a theoretical reference for the subsequent optimization of TCL-based immunotherapeutic strategies.

Acknowledgements: This research was supported by National Natural Science Foundation of China Youth Fund Project (81402351), Anhui Province University Outstanding Young Talent Support Program (Key Program) (gxyqZD2019040), Project of Outstanding Talents of Wannan Medical College (wyqnyx202001), and Natural Science Research Project of Anhui Provincial Department of Education (Major Projects) (2023AH040263).

REFERENCES

1. Fahad Ullah M (2019) Breast cancer: Current perspectives on the disease status. *Adv Exp Med Biol* **1152**, 51–64.
2. Zhu Y, Ren J, Wu X, Zhang Y, Wang Y, Xu J, Tan Q, Jiang Y, et al (2023) lncRNA ENST00000422059 promotes cell proliferation and inhibits cell apoptosis in breast cancer by regulating the miR-145-5p/KLF5 axis. *Acta Biochim Biophys Sin* **55**, 1892–1901.
3. Chen WQ, Zheng RS (2015) Incidence, mortality and survival analysis of breast cancer in China. *Chin J Clin Oncol* **42**, 668–674.
4. Zhang J, Pan S, Han C, Jin H, Sun Q, Du J, Han X (2022) Combination of immune-related network and molecular typing analysis defines a three-gene signature for predicting prognosis of triple-negative breast cancer. *Biomolecules* **12**, 1556.
5. Zhu Y, Zhu X, Tang C, Guan X, Zhang W (2021) Progress and challenges of immunotherapy in triple-negative breast cancer. *Biochim Biophys Acta Rev Cancer* **1876**, 188593.
6. Sun M, Guo H (2023) Role of autophagy-mediated miR-18a in breast cancer progression *in vitro*. *ScienceAsia* **49**, 177–183.
7. Kitamura H, Ohno Y, Toyoshima Y, Ohtake J, Homma S, Kawamura H, Takahashi N, Taketomi A (2017) Interleukin-6/STAT3 signaling as a promising target to improve the efficacy of cancer immunotherapy. *Cancer Sci* **108**, 1947–1952.
8. Zuo S, Huang Y, Zou J (2024) The role of the gut microbiome in modulating immunotherapy efficacy in colorectal cancer. *IUBMB Life* **76**, 1050–1057.
9. Chen Z, Liu W, Yang Z, Luo Y, Qiao C, Xie A, Jia Q, Yang P, et al (2023) Sonodynamic-immunomodulatory nanostimulators activate pyroptosis and remodel tumor microenvironment for enhanced tumor immunotherapy. *Theranostics* **13**, 1571–1583.
10. Javed SA, Najmi A, Ahsan W, Zoghebi K (2024) Targeting PD-1/PD-L-1 immune checkpoint inhibition for cancer immunotherapy: Success and challenges. *Front Immunol* **15**, 1383456.
11. Li T, Niu M, Zhou J, Wu K, Yi M (2024) The enhanced antitumor activity of bispecific antibody targeting PD-1/PD-L1 signaling. *Cell Commun Signal* **22**, 179.
12. Xu Z, Shen J, Wang MH, Yi T, Yu Y, Zhu Y, Chen B, Chen J, et al (2016) Comprehensive molecular profiling of the B7 family of immune-regulatory ligands in breast cancer. *Oncoimmunology* **5**, e1207841.
13. Jiang X, Wang J, Deng X, Xiong F, Ge J, Xiang B, Wu X, Ma J, et al (2019) Role of the tumor microenvironment in PD-L1/PD-1-mediated tumor immune escape. *Mol Cancer* **18**, 10.
14. Yi M, Niu M, Xu L, Luo S, Wu K (2021) Regulation of PD-L1 expression in the tumor microenvironment. *J Hematol Oncol* **14**, 10.
15. Jin Y, Mu Y, Zhang S, Li P, Wang F (2020) Preparation and evaluation of the adjuvant effect of curdlan sulfate in improving the efficacy of dendritic cell-based vaccine for antitumor immunotherapy. *Int J Biol Macromol* **146**, 273–284.
16. Ribas A, Wolchok JD (2018) Cancer immunotherapy using checkpoint blockade. *Science* **359**, 1350–1355.
17. Powles T, Eder JP, Fine GD, Braiteh FS, Loriot Y, Cruz C, Bellmunt J, Burris HA, et al (2014) MPDL3280A (anti-PD-L1) treatment leads to clinical activity in metastatic bladder cancer. *Nature* **515**, 558–562.
18. Gao Y, Nihira NT, Bu X, Chu C, Zhang J, Kolodziejczyk A, Fan Y, Chan NT, et al (2020) Acetylation-dependent regulation of PD-L1 nuclear translocation dictates the efficacy of anti-PD-1 immunotherapy. *Nat Cell Biol* **22**, 1064–1075.
19. Uhercik M, Sanders AJ, Owen S, Davies EL, Sharma AK, Jiang WG, Mokbel K (2017) Clinical Significance of PD1 and PDL1 in Human Breast Cancer. *Anticancer Res* **37**, 4249–4254.
20. Wang Z, Zhu M, Dong R, Cao D, Li Y, Chen Z, Cai J, Zuo X (2023) TH-302-loaded nanodrug reshapes the hypoxic tumour microenvironment and enhances PD-1 blockade efficacy in gastric cancer. *J Nanobiotechnol* **21**, 440.
21. Gil Del Alcazar CR, Huh SJ, Ekram MB, Trinh A, Liu LL, Beca F, Zi X, Kwak M, et al (2017) Immune escape in breast cancer during *in situ* to invasive carcinoma transition. *Cancer Discov* **7**, 1098–1115.
22. Mittendorf EA, Philips AV, Meric-Bernstam F, Qiao N, Wu Y, Harrington S, Su X, Wang Y, et al (2014) PD-L1 expression in triple-negative breast cancer. *Cancer Immunol Res* **2**, 361–370.

23. Akiki M, Haddad FG, Kourie HR, Khaddage A, Smayra VT (2019) PD-L1: An unavoidable biomarker in advanced triple-negative breast cancer. *Biomark Med* **13**, 1539–1541.
24. Barrett MT, Anderson KS, Lenkiewicz E, Andreozzi M, Cunliffe HE, Klassen CL, Dueck AC, McCullough AE, et al (2015) Genomic amplification of 9p24.1 targeting JAK2, PD-L1, and PD-L2 is enriched in high-risk triple negative breast cancer. *Oncotarget* **6**, 26483–26493.
25. Guo L, Li W, Zhu X, Ling Y, Qiu T, Dong L, Fang Y, Yang H, et al (2016) PD-L1 expression and CD274 gene alteration in triple-negative breast cancer: implication for prognostic biomarker. *SpringerPlus* **5**, 805.
26. Balko JM, Giltnane JM, Wang K, Schwarz LJ, Young CD, Cook RS, Owens P, Sanders ME, et al (2014) Molecular profiling of the residual disease of triple-negative breast cancers after neoadjuvant chemotherapy identifies actionable therapeutic targets. *Cancer Discov* **4**, 232–245.
27. Xiong W, Gao Y, Wei W, Zhang J (2021) Extracellular and nuclear PD-L1 in modulating cancer immunotherapy. *Trends Cancer* **7**, 837–846.
28. Parra ER, Villalobos P, Rodriguez-Canales J (2019) The multiple faces of programmed cell death ligand 1 expression in malignant and nonmalignant cells. *Appl Immunohistochem Mol Morphol* **27**, 287–294.
29. Wan X, Fang M, Chen T, Wang H, Zhou Q, Wei Y, Zheng L, Zhou Y, et al (2022) The mechanism of low-dose radiation-induced upregulation of immune checkpoint molecule expression in lung cancer cells. *Biochem Biophys Res Commun* **608**, 102–107.
30. Hou J, Zhao R, Xia W, Chang CW, You Y, Hsu JM, Nie L, Chen Y, et al (2020) PD-L1-mediated gasdermin C expression switches apoptosis to pyroptosis in cancer cells and facilitates tumour necrosis. *Nat Cell Biol* **22**, 1264–1275.
31. Liu Y, Yang Z, Wang S, Miao R, Chang CM, Zhang J, Zhang X, Hung MC, et al (2024) Nuclear PD-L1 compartmentalization suppresses tumorigenesis and overcomes immunocheckpoint therapy resistance in mice via histone macroH2A1. *J Clin Invest* **134**, e181314.
32. Ghebeh H, Lehe C, Barhoush E, Al-Romaih K, Tulbah A, Al-Alwan M, Hendrayani SF, Manogaran P, et al (2010) Doxorubicin downregulates cell surface B7-H1 expression and upregulates its nuclear expression in breast cancer cells: role of B7-H1 as an anti-apoptotic molecule. *Breast Cancer Res* **12**, R48.
33. Nihira NT, Ogura K, Shimizu K, North BJ, Zhang J, Gao D, Inuzuka H, Wei W (2017) Acetylation-dependent regulation of MDM2 E3 ligase activity dictates its oncogenic function. *Sci Signal* **10**, eaai8026.
34. Chen ZY, Wang L, Gu L, Qu R, Lowrie DB, Hu Z, Sha W, Fan XY (2020) Decreased expression of CD69 on T cells in tuberculosis infection resisters. *Front Microbiol* **11**, 1901.
35. Seropian IM, Cerliani JP, Toldo S, Van Tassell BW, Ilarregui JM, González GE, Matoso M, Salloum FN, et al (2013) Galectin-1 controls cardiac inflammation and ventricular remodeling during acute myocardial infarction. *Am J Pathol* **182**, 29–40.
36. Prompoon Y, Yurasakpong L, Suwannakhan A, Chawiwithaya C, Chotwiwatthanakun C, Weerachatyanukul W, Nantasenamat C, Asuvapongpatana S (2024) Betulinic acid inhibits proliferation and triggers apoptosis in human breast cancer cells by modulating ER (α/β) and p53. *ScienceAsia* **50**, 2024085.
37. Sreejit G, Abdel-Latif A, Athmanathan B, Annabathula R, Dhyani A, Noothi SK, Quaife-Ryan GA, Al-Sharea A, et al (2020) Neutrophil-derived S100A8/A9 amplify granulopoiesis after myocardial infarction. *Circulation* **141**, 1080–1094.
38. Pinelli E, Killick-Kendrick R, Wagenaar J, Bernadina W, del Real G, Ruitenberg J (1994) Cellular and humoral immune responses in dogs experimentally and naturally infected with *Leishmania infantum*. *Infect Immun* **62**, 229–235.
39. Marabondo S, Kaufman HL (2017) High-dose interleukin-2 (IL-2) for the treatment of melanoma: Safety considerations and future directions. *Expert Opin Drug Saf* **16**, 1347–1357.
40. Chang WK, Yang KD, Shaio MF (1999) Effect of glutamine on Th1 and Th2 cytokine responses of human peripheral blood mononuclear cells. *Clin Immunol* **93**, 294–301.
41. Zhang Y, Zhu L, Li X, Ge C, Pei W, Zhang M, Zhong M, Zhu X, et al (2024) M2 macrophage exosome-derived lncRNA AK083884 protects mice from CVB3-induced viral myocarditis through regulating PKM2/HIF-1α axis mediated metabolic reprogramming of macrophages. *Redox Biol* **69**, 103016.
42. Li Y, Gu R, Yan F, Liu Z, Zhang X, Zhao X, Xu F (2024) Low-dose atorvastatin calcium combined with evolocumab: Effect on regulatory proteins, lipid profiles, and cardiac function in coronary heart disease patients. *Am J Transl Res* **16**, 2334–2345.
43. Calcagno AM, Fostel JM, To KKW, Salcido CD, Martin SE, Chewning KJ, Wu CP, Varticovski L, et al (2008) Single-step doxorubicin-selected cancer cells overexpress the ABCG2 drug transporter through epigenetic changes. *Br J Cancer* **98**, 1515–1524.